Detecting instant of multiple faults on transmission line and its types using time-frequency analysis

Shweta[1], Nand Kishor[1*], Kjetil Uhlen[2], Soumya Ranjan Mohanty[3]

[1]Department of Electrical Engineering, Motilal Nehru National Institute of Technology Allahabad, India
[2]Department of Power Engineering, NTNU, Trondheim, Norway
[3]Department of Electrical Engineering, IIT BHU, Varanasi, India
[*]E-mail: nand_research@yahoo.co.in

Abstract: In a complex interconnected network, due to dynamic interaction between the AC networks, at the time of multiple occurrences of faults, the successful relay operation is threatened. For security and reliability of power system network, fast and accurate protection scheme is of great importance. This paper presents a protection scheme for multiple faults detection at bus/line and its type in wide area network. If a fault occurs on a line, followed by another fault at the same/different line, before the clearance of former fault, the proposed scheme is capable to detect such multiple fault events. The protection scheme applies processed signal information for its time-frequency representation using Smoothed Pseudo Wigner-Ville distribution, followed by Hilbert transform and calculation of indices to interpretate the fault events. It is shown that faulted bus, faulted line, time instant, and types of fault can be easily identified without involving any high computationally burden. The proposed scheme is validated on the signals simulated on two area Kundur's model and standard IEEE 39 bus system and verified with real-time signals on RTDS for different fault conditions; fault resistance and fault location on the line. The scheme can be successfully applied on wide area signals available from PMUs for wide area network protection.

Keywords: Multiple faults, Detection, Time-frequency representation

1. Introduction

Detection of the fault location in transmission line is one of the vital concern for power system security. Due to rapid growth in the technology to make the grid smarter, the use of synchrophasors for power system has widen the geographical area. Synchrophasor technology offers a great future for dynamic supervision, protection and control of wide-area power system. The Phasor Measurement Unit (PMU) is a data acquisition system, realized through a digital recording device.

Different transient events like faults, line switching, switching on/off of heavy loads, generator disconnection etc. do occur in the power system. Among these, quick and accurate detection of faults is important to avoid any cascading outages. To accelerate the repair and restoration of power supply, it is essential to know the complete information about the fault or if not known then must be estimated from the PMUs data with an acceptable accuracy [1] - [3].

In last one decade, several techniques have been reported on fault detection and classification using signal processing techniques, including artificial intelligence. The use of Support Vector Machine (SVM) and Principal Component Analysis (PCA) techniques, with different window sizes have been proposed in [4] for detection and classification of fault conditions. An improvement in classification accuracy, combined with wavelet transform was suggested in [5]. Wavelet transform has been also combined with different entropies [6]. The wavelet transform applied on three phase current signals at sending end of line and using statistical decision-tree for classification was reported in [7]. Artificial Neural Networks (ANN), which have been widely studied for fault detection and classification, require a training process and need one cycle of information to classify events [8]. Fault identification was also addressed using fuzzy techniques [9-10]. Such methods do not require a training process, however their generalization is more complex. The fault classification using moving sum of current signals was proposed in [11] and it was discussed that the moving sum remains non-zero during fault or transient conditions.

Most of the works based on PMUs data are concentrated on identification of fault location [12] – [18]. The travelling wave based method has been proposed [12], which was claimed to be immune to system parameters, but it requires very high sampling frequency and faces difficulty to discriminate between faulty and non-faulty measurements. Maximum Wavelet Singular Value (MWSV) calculated through Discrete Wavelet Transform (DWT) for a sliding window was discussed in [13]. Exceeding the value of MWSV above predefined threshold indicates the occurrence of fault. With a delay of 5 msecs, the Euclidean norm of MWSV was computed and compared with the set value, based on which the faults are classified. Das et al. [14] suggested that the change in injected current at the faulted bus is non-zero while at non-faulted bus it is zero. A voltage magnitude (VM) based approach has been discussed in [15], to identify the faulty bus. Further, faulty line has been identified by comparing the angle of positive sequence current of all the connected lines to the faulty bus. Similar concept has been introduced in [16], except the use of sequence component of voltage and current phasors. The study [17] presented use of only voltage phasor to identify the fault. The scheme works in three folds; first to identify the fault region, second to identify faulted feeder and lastly backup protection. Based on the level of voltage depression and recovery, identification of fault is analysed. Such economical approaches are fast and accurate.

The literatures available have mainly discussed the study related to fault identification and classification limited to single fault occurrence at a time, but not to multiple events. In recent years, fault diagnosis has been investigated involving the consequences during fault scenarios, for example, power swing that affects the relay operation. Such studies have been reported in [18] for uncompensated and compensated line [19]. The study [20] used Koopman mode analysis (KMA), for multiple faults diagnosis. The

technique involving calculation of a threshold and rule base is reported in [21], however, the calculation of threshold is tedious task and perhaps cannot be generalized. The authors [22] proposed the use of FFT coefficient from equivalent voltage/current phasor angle to detect the fault. It can reliably detect the fault but for simultaneous faults, it shows error and it takes *1/f* time period to detect the fault. Recently, authors [23] proposed Power Spectral Density (PSD) based approach to detect and classify the faults on transmission line. The current signals are scaled using DWT in time and frequency domain at different decomposition levels. The obtained coefficients are used to form a wavelet covariance matrix. However, the decision about the fault and its classification remains predefined threshold value based.

In interconnected network, on occurrence of an event, the propagation of dynamic transient due to dynamic interactions between the AC systems can be observed [24]. It is clear that with wide area measurements available from the bus, it is more important to achieve accurate and reliable detection of multiple faults that has occurred in the system in subsequent instant. Due to superimposition of signals available at the buses, it is more challenging to detect the faults, which occurs in one line following another line. In other words, the transient signal due to fault event in one of the line is more likely to propagate to another line and this situation becomes worse if another fault initiates before the former has cleared. This problem further aggregates if the fault is of different types in the subsequent instant of its occurrence. The failure in discrimination of such fault events is likely to lead maloperation of relays.

Main contribution of proposed scheme lies in the fact that it is oriented to detect multiple faults occurrence within time duration of 10 msec. It is capable to detect those events that involve occurrence of one fault, followed by another fault on the same line or nearby line. Fault detection is successful even for different fault conditions like fault types; LG, LLL, LL occurrence on different lines, fault resistance and fault location. The noise in range of 20 dB – 50 dB SNR in the signals corresponding to interarea modes (0 – 1Hz) has been considered to detect coherency [25]. The reported scheme gives satisfactory results and have a high noise tolerance. Thus, it is important to validate any scheme that uses real-life PMU data measurements associated with noisy signals.

In this paper, the proposed algorithm presents an approach to detect the multiple faults occurrence using advanced signal processed information. The voltage/current phasor of all the three phases available from the bus are processed into Pseudo voltage phasor angle (PVPA), positive sequence components and mean voltage deviation. Subsequently on PVPA signal, change in time-frequency spectra (CTFS) index is calculated using Smoothed Pseudo Wigner-Ville distribution (SPWVD) from time-frequency (TF) representation. This index is used to detect the bus near to the fault point and instant of its occurrence. Applying Hilbert transform on the voltage deviation signal of each phase of the faulted bus, results into complex form. The cluster formed from the scatter plot of absolute and imaginary components of complex value help in detecting the type of fault. Then, Total Spectra Coefficient (TSC) index is evaluated using SPWVD, for each connecting lines from the faulted bus to identify the faulty line. The proposed scheme for multiple faults detection is first tested on a simple two area system (Kundur's model) and further its validation is carried out on complex interconnected network. The study is compared with FFT method [22]. Further, the efficacy of fault detection algorithm is tested using real time measurement on real time digital simulator (RTDS). It is shown that subsequent fault occurrence (multiple faults before the clearance of former fault) can be easily detected using the signal from the bus associated with fault line. The detection remains accurate and reliable even if there exists superposition of signal at the bus due to fault occurrence at one of line and another fault initiates (before the former fault has cleared) on adjoining line that connects to the same bus. The performance remains unaffected with the types of fault that occurs in subsequent instants.

The paper is arranged as follows. The proposed methodology is briefly explained in Section 2, followed by adoption of techniques in the algorithm is explained in Section 3. The verification of proposed methodology is discussed in Section 4. Finally, the conclusions are given in Section 5.

2. Proposed Methodology

In this section, we discuss the techniques in details, which are used in the proposed approach.

2.1. Signal Transformation

2.1.1 Pseudo Voltage Phasor Angle (PVPA): The fault occurrence results into maximum transient variation in voltage and current signals for the faulted bus/line. As such, these signals can be considered as working signal for fault diagnosis. The three phase voltage signals, V_R, V_Y and V_B from PMUs can be converted into two-phase orthogonal quantities; d and q components, i.e. V_d and V_q using Park's transformation. The Pseudo Voltage Phasor Angle is calculated as:

$$\varphi_v = tan^{-1}\left(\frac{V_q}{V_d}\right) \tag{1}$$

The PVPA (φ_v) at all the buses is determined with respect to one of the generator bus which is considered as a reference bus. It is clear, this PVPA will remain constant for healthy condition of the bus and on fault occurrence, a high frequency component can be observed. As such, TF representation can be performed on the change in PVPA (CPVPA) signal, i.e. $\Delta\varphi_v(t)$, which indicates about the energy content in the signal with respect to time and frequency. Obviously, the bus near to fault point has highest energy content, which is denoted by change in Time Frequency Spectra (CTFS) index.

2.1.2 Positive Sequence Current: Symmetrical components are used to simplify fault analysis by converting a three-phase unbalanced signal into symmetrical components. These sets of components are called the positive, negative, zero-sequence components and for current signal, it is calculated as:

$$\begin{bmatrix} I_0 \\ I_1 \\ I_2 \end{bmatrix} = \frac{1}{3}\begin{bmatrix} I_R + I_Y + I_B \\ I_R + \alpha I_Y + \alpha^2 I_B \\ I_R + \alpha^2 I_Y + \alpha I_B \end{bmatrix} \tag{2}$$

where $\alpha = e^{\frac{2\pi i}{3}}$, I_0, I_1 and I_2 is zero, positive and negative sequence component respectively. Mainly, the positive sequence current is of interest, which can accurately inform about the faulty line.

2.1.3 Mean Voltage deviation: The three-phase mean voltage deviation (ΔV_m) at k^{th} bus with respect to previous sliding window can be calculated from:

$$\Delta V_{m,k} = \frac{|\Delta V_{R,k}|+|\Delta V_{Y,k}|+|\Delta V_{B,k}|}{3} \quad (3)$$

where $\Delta V_{R,k}$ is the voltage deviation for R phase

$\Delta V_{R,k} = V_{R,k}((n+1)^{th}) - V_{R,k}((n)^{th})$, n = sample

Whenever fault occurs, the mean voltage deviation of the bus sharing the faulted line will show highest absolute value. All the three phases are involved in mean voltage, which will result in higher threshold value (for any fault, transient appear in all phases). This is another analytics to confirm presence of fault in the network.

2.2. Signal Processing

2.2.1 Smoothed pseudo Wigner-Ville distribution (SPWVD): To characterise the power quality of a non-stationary signal, TF analysis has emerged as a powerful tool. There are two methods; linear and bilinear. The former method has less computational complexity but at the cost of TF resolution. The disadvantage associated with bilinear methods is typical interface called cross-terms. SPWVD is a bilinear method featured by a separable kernel, which allows smoothing to be adjusted independently for both time and frequency, hence becomes one of the most flexible Cohen's class TF distributions. The TF representation of non-stationary signal of CPVPA i.e., $\Delta\varphi_v(t)$ using Wigner-Ville spectrum is given as [26]:

$$\mathfrak{S}_{\Delta\varphi_v\Delta\varphi_v}(t,f) = \mathfrak{F}_{\tau\to f}\{\mathfrak{E}\left[\Delta\varphi_v\left(t+\frac{\tau}{2}\right)\Delta\varphi_v{}^*\left(t-\frac{\tau}{2}\right)\right] \quad (4)$$

where $\mathfrak{E}$ [.] stands for expectation operator and $\mathfrak{F}$ {.} stands for Fourier transform.

On certain conditions, the Wigner-ville spectrum (WVS) is ensemble average of the Wigner-Ville distribution, $\grave{\mathrm{W}}_{\Delta\varphi_v\Delta\varphi_v}(t,f)$ of the realizations of the signal [21].

$$\mathfrak{S}_{\Delta\varphi_v\Delta\varphi_v}(t,f) = \mathfrak{E}\left[\grave{\mathrm{W}}_{\Delta\varphi_v\Delta\varphi_v}(t,f)\right] \quad (5)$$

$$\grave{\mathrm{W}}_{\Delta\varphi_v\Delta\varphi_v}(t,f) = \mathfrak{F}_{\tau\to f}\left[\Delta\varphi_v\left(t+\frac{\tau}{2}\right)\Delta\varphi_v{}^*\left(t-\frac{\tau}{2}\right)\right] \quad (6)$$

$\mathfrak{S}_{\Delta\varphi_v\Delta\varphi_v}(t,f)$ can be estimated via local averaging.

$$\mathfrak{S}_{\boldsymbol{\Delta\varphi_v\Delta\varphi_v}}(\boldsymbol{t},\boldsymbol{f};\,\boldsymbol{\theta}) = \grave{\mathrm{W}}_{\boldsymbol{\Delta\varphi_v\Delta\varphi_v}}(\boldsymbol{t},\boldsymbol{f}) \otimes \boldsymbol{\theta}(\boldsymbol{t},\boldsymbol{f}) \quad (7)$$

where, $\otimes$ is the convolution on $\boldsymbol{t}$ and $\boldsymbol{f}$, and $\boldsymbol{\theta}(\boldsymbol{t},\boldsymbol{f})$ is a smoothing function.

The Smoothed Pseudo Wigner-Ville distribution (SPWVD) [27] for processed CPVPA signal is given as:

$$\mathfrak{S}^{W}_{\Delta\varphi_v\Delta\varphi_v}(t,f) = \grave{\mathrm{W}}_{\Delta\varphi_v\Delta\varphi_v}(t,f) \otimes \theta(t,f)$$

$$\mathfrak{S}^{W}_{\Delta\varphi_v\Delta\varphi_v}(t,f) = \mathfrak{F}_{(v,\tau)\to(t,f)}\{\mathcal{A}_{\Delta\varphi_v\Delta\varphi_v}(v,\tau)\vartheta(v,\tau)\}$$

$$\mathcal{A}_{\Delta\varphi_v\Delta\varphi_v}(v,\tau) = \mathfrak{F}_{t\to v}\{\Delta\varphi_v\left(t+\frac{\tau}{2}\right)\Delta\varphi_v{}^*\left(t-\frac{\tau}{2}\right)\}$$

$$\vartheta(v,\tau) = \mathfrak{F}^{-1}_{(t,f)\to(v,\tau)}\{\theta(t,f)\} \quad (8)$$

where, $\mathfrak{F}_{(v,\tau)\to(t,f)}$ is the Fourier transform, passing the ambiguity function domain to TF domain and $\mathcal{A}_{\Delta\varphi_v\Delta\varphi_v}(v,\tau)$ is the ambiguity function of $\Delta\varphi_v(t)$.

A simple version of multiform-tiltable exponential kernel [28] is used, to suppress the interference terms.

$$\vartheta(v,\tau) = \exp\left\{-\pi\left[\left(\frac{v}{v_0}\right)^2+\left(\frac{\tau}{\tau_0}\right)^2\right]^{2\lambda}\right\} \quad (9)$$

The TF spectra coefficient and Change in Time Frequency Spectra (CTFS) is calculated using (8). The information contained in the TF spectra signifies about the energy content of particular frequency at that instant. Hence, the bus which shares the faulted line is expected to indicate higher energy content.

Similarly, the deviation in positive sequence line current ($\Delta I(t)$) can be considered as working signal and so, the TF spectra becomes $\mathfrak{S}_{\Delta I\Delta I}(t,f)$. The Total Spectra Coefficient (TSC) is determined as:

$$TSC = \sum_{f=0}^{f=\frac{f_s}{2}} \mathfrak{S}_{\Delta I\Delta I}(t,f) \quad (10)$$

where, f_s is the sampling frequency.

Higher TSC value among the lines indicates faulty line.

2.2.2 Hilbert Transform (HT): The Hilbert Transform defined on real signal $\Delta V_{i,k}(t)$ where *i= R, Y* and *B* phase are extended into the complex plane such that it satisfies the Cauchy–Riemann equations. It extracts instantaneous information of amplitude and phase. It refers to the following equations:

$$H\left(\Delta V_{i,k}(t)\right)(t) = \frac{1}{\pi} P \int_{-\infty}^{\infty} \frac{\Delta V_{i,k}(t)}{t-\tau}\, d\tau \quad (11)$$

$$\Delta V_{i,k_a}(t) = \Delta V_{i,k}(t) + j.H\left(\Delta V_{i,k}(t)\right)(t) \quad (12)$$

Now, evaluate absolute and imaginary component from eqn. (12) for voltage deviation signal of all three phases. The scatter plot of these features (components) will form clusters for fault signals involving particular phase. The types of fault will affect the pattern representation of clusters, i.e. faulty phase features will be located away from the origin in absolute and imaginary plane as discussed in Section 4. This helps in identifying the fault types.

3. Algorithm

This section presents the discussion on application of above discussed techniques for fault diagnosis in the power system. The objective of diagnosis lies in three folds; i) detect the faulted bus, ii) its type and iii) identify the faulted line. The proposed method in the form of flow chart is presented in Fig. 1.

The signals; three phase voltage and current are sampled from PMU on a base frequency of 50 Hz, having a sampling rate of 1kHz. This results in 1000 samples in 1 sec (i.e. 50 cycles) and the algorithm runs on a sliding window of 100 samples, with 90% overlap. It means during each iteration of proposed algorithm, 10 new samples are included in analysis window. The computational time taken by the algorithm to take decision about the characteristic of fault and its location is 9.54 msec, so the fault occurrence is detected within 10 msec. In the first step, mean voltage deviation, $\Delta V_{m,k}$ is calculated for all the buses, wherein k denotes the buses. A threshold value 0.015 is determined by considering the condition of least severe fault that could be possible in the network. The bus connecting the line with fault occurrence is now determined from:

Fault bus j, $\Delta V_{m,j}$= max ($\Delta V_{m,k}$) (13)

The three phase voltage signals from the corresponding bus are used to determine the type of fault. The HT is applied on the mean voltage deviation signal of each phase and their absolute and imaginary components is plotted.

Further, the TF representation using SPWVD is analysed on positive sequence line current signals. The maximum value of TSC calculated for all the lines that connects the fault bus suggests the fault line.

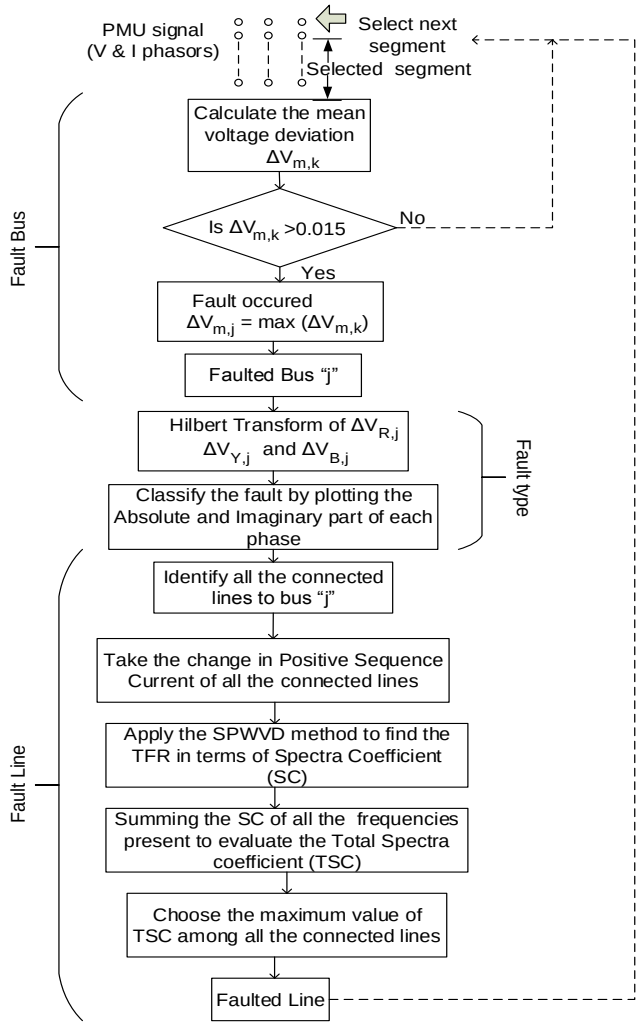

Fig. 1. *Flow chart of the algorithm*

4. Verification of the Proposed Approach

The above described methodology for fault diagnosis is performed on IEEE standard power system network models simulated on MATLAB/Simulink R2013a platform.

4.1. Test System

Fig. 2(a) depicts the single line diagram of two area Kundur's model that consists of 4 machines (G1-G2 belong to area 1 & G3-G4 to area 2) and under normal operating condition, power flows from area 1 to area 2.

The detailed model of machines including the control parameters are simulated [29]. PMUs are assumed to be installed at bus 5 to bus 11. The well-known IEEE 39 bus test system [30] is also considered that consists of 39 buses with 10 generators.

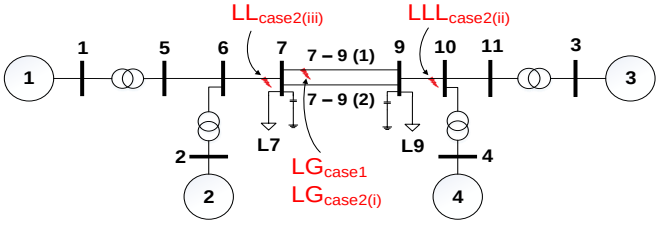

(a) Two area Kundur's model

Fig. 2(b) shows the single line diagram of said bus system. The details on description of multiple faults simulated in study and as shown in Fig. 2 is discussed in next section.

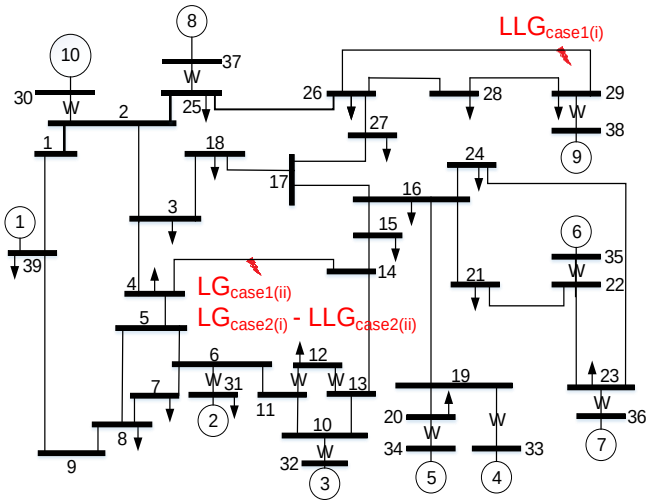

(b) IEEE 39 bus system

Fig. 2. *Test systems*

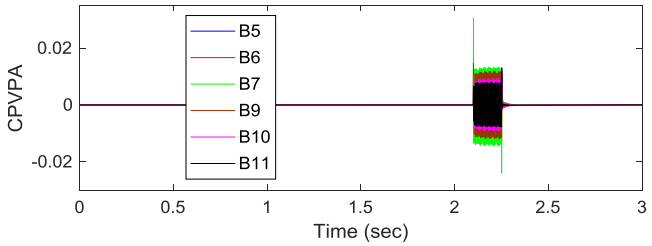

(a) CPVPA at all buses

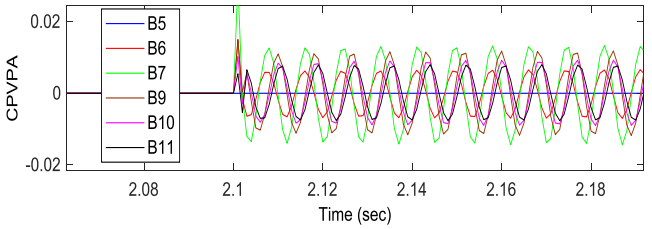

(b) Zoomed plot of CPVPA variation

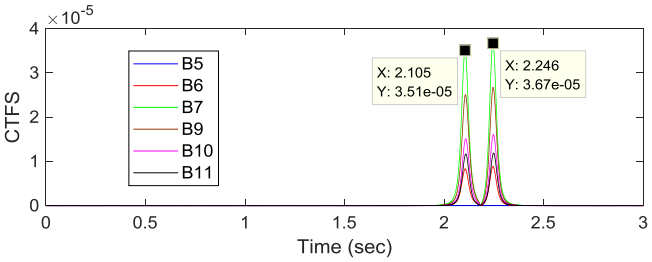

(c) CTFS at buses

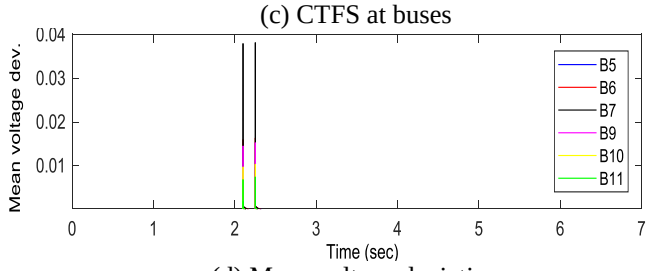

(d) Mean voltage deviation

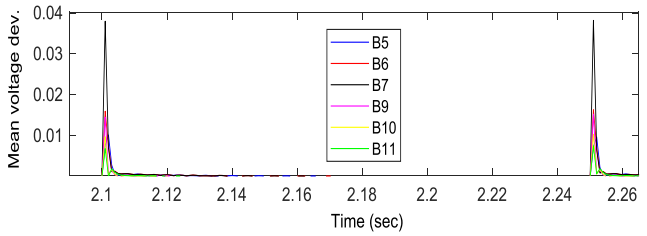

(e) Zoomed plot of mean voltage deviation

Fig. 3. *Fault bus indenfication*

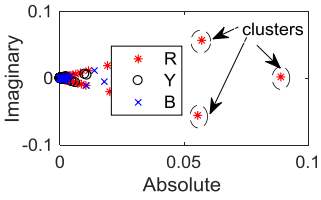

(a) LG(R-G) fault near Bus7

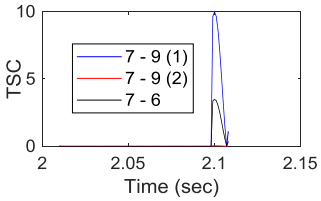

(b) TSC of connecting lines

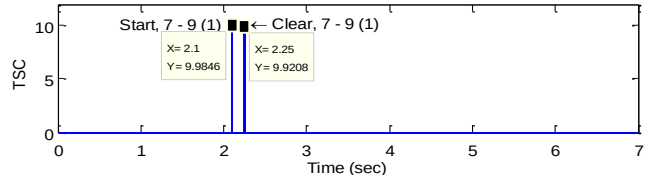

(c) Fault at line 7 - 9 (1) and its timing

Fig. 4. *Detection of fault type and its duration for case 1 in two area system*

4.2 Two Area Kundur's Model

First, in study, the performance of proposed approach is investigated on a simple two area network. The different case studies are performed for fault created on the lines that connects the two areas.

Case 1: *Single instant of fault occurrence* (LG_{case1})- A single line to ground (LG) fault with a fault resistance (R_f) 100 Ω is created on transmission line (1) that connects the buses; 7 – 9, i.e. 7 - 9(1), at 23% distance from the bus 7. The fault occurs at t = 2.1 sec and allowed to get cleared at t = 2.25 sec.

The variation in CPVPA at all buses during the fault duration in the analysis window can be seen in Fig. 3(a)-(b). The maximum value of CTFS is indicated for bus 7 as observed in Fig. 3(c). This suggests bus 7 shares the line with fault occurrence. It is also confirmed from the variation of mean voltage deviation as observed in Fig. 3(d)-(e). Now, the fault type and fault line are investigated and shown in Fig. 4. The scattered absolute and imaginary components obtained from HT corresponding to R-phase in Fig. 4(a) suggests the LG fault type. The phase that involves fault has its distribution of features (HT) in the form of clusters located away from the origin of the plot. The fault associated to bus 7 connects multiple circuits with bus 9 and a line with bus 6, but the total spectra coefficient calculated for signals further confirms the fault occurrence on line 7 - 9(1). The fault duration with information on fault initiation and its clearance can be observed in Fig. 4(c), shown as sliding window (100 samples) with 90% overlapping of the previous window for complete duration of signal. The performance of proposed method is further validated for different conditions and given in Table 1. The no fault condition indicates zero value of TSC. As from the flow chart, it is clear that the mean voltage deviation is less than 0.015 value for each iteration and hence the TSC index remain zero, indicating no fault case. It is understood the value of TSC satisfactorily indicates the fault occurrence in the line.

Table 1 *TSC for all the connected lines in two area Kundur's model*

Fault details	Fault Bus	Connected Lines	TSC
(i) No fault	-	-	0
(ii) LL fault in 7 - 9 (1), 10 % distance from bus 7, R_f =100 Ω	7	**7 – 9 (1)**	**63.89**
		7 – 9 (2)	35.08
		7 - 6	0.3494
(iii) LLL fault in 7 - 9 (2), 50 % distance from bus 7, R_f =0.001 Ω	9	7 – 9 (1)	0.9358
		7 – 9 (2)	**444.2**
		9 - 10	13.77
(iv) LLG fault in 6 - 7, 90 % distance from bus 6, R_f =200 Ω	6	**6 – 7**	**15.24**
		5 - 6	3.539
(v) LG fault in 9 - 10, 10 % distance from bus 9, R_f =50 Ω	9	7 – 9 (1)	0.2432
		7 – 9 (2)	0.2433
		9 - 10	**36.4**

Case 2: Multiple instants of fault occurrence- This case is investigated for simultaneous occurrence of faults of different types in the network. In other words, the network (line) experiences one type of fault and meanwhile another type of fault is initiated before the first fault has cleared. The following multiple fault events (Fig. 2(a)) are created to test the proposed approach:

(i) First event: $LG_{case2(i)}$(R-G) fault with a fault resistance 0.01Ω on line 7 - 9(1) at 23% distance from bus 7, occurs at t = 1 sec and cleared at t = 1.3 sec.

(ii) Second event: $LLL_{case2(ii)}$ fault with a fault resistance 200Ω on line 10 -9, at 10% distance from bus 10, occurs at t = 1.15 sec and clears at t = 1.4 sec.

(iii) Third event: $LL_{case2(iii)}$ (R-Y) fault with a fault resistance 100Ω on line 6 - 7, at 90% distance from bus 6, occurs at t = 2.0 sec and clears at t = 2.15 sec.

From Fig. 5(a), the fault associated bus is clearly evident. The absolute and imaginary components calculated for signal from bus 7 suggests the scatter corresponding to R-phase only, i.e. LG fault. This is evident from Fig. 5(b)(i). The phase (R) involving fault has separated out from the features of healthy (Y & B), mainly concentrated near origin axis. Further, as an example in Fig. 5(b)(ii), the TSC plot for first event also suggests the fault occurrence on the line 7 - 9(1). The fault type for second and third events as illustrated in Fig. 5(b)(iii) & (iv) indicates LLL and LL fault respectively. The scatter of HT for all three phases are together in a cluster for LLL type fault, while for LL type, the phases involved in fault are scattered apart from the healthy phase.

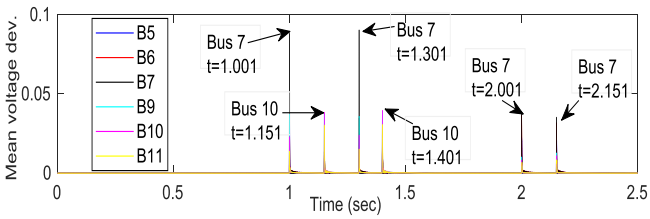

(a) Fault bus identification

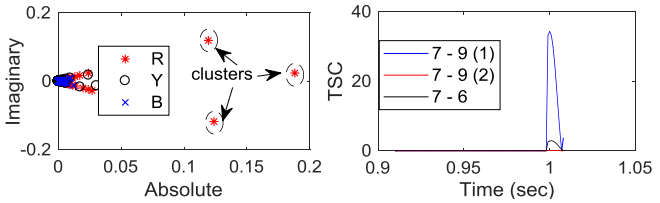

(i) First Event (LG) (ii) TSC of all lines for first event

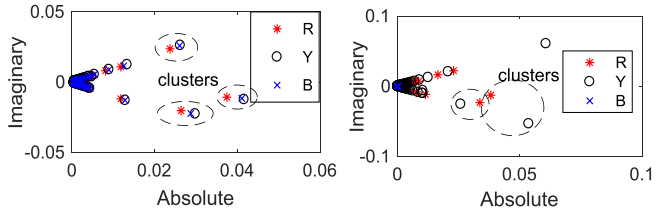

(iii) Second event (LLL) (iv) Third event (LL)

(b) Fault types detection

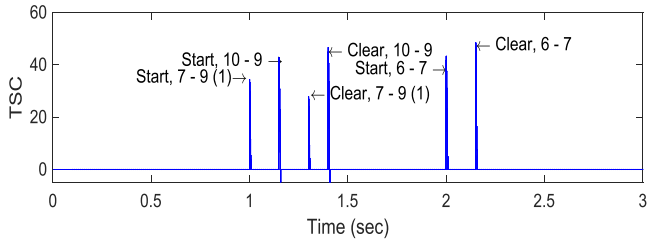

(c) Multiple faults sequence on different lines

Fig. 5. *Detection of multiple faults*

With LL fault (R, Y phases), overlapping between clusters involving R, Y phases are clearly visible, while B phase which is healthy is concentrated at origin. In other words, with LL type fault, the HT is seen to have wide spread scatter for the phase undergoing fault. The scatter of absolute and imaginary components corresponding to all three phases remain in same cluster with respect to each other for LLL fault in contrast to LL fault wherein, due to unsymmetrical cluster between faulty phases is not formed. The detection of multiple faults is successfully shown in Fig. 5(c). It is clear that simultaneous faults of different types can be accurately detected, including their instant of occurrence and clearance. The proposed methodology applied on sliding window indicates the instant of first event on line 7 - 9(1) and also reliably suggests the second event on line 10 - 9, before the former fault has cleared. It is to mention here the value of TSC for each fault events depends on several factors; its severeness, fault location, fault type and fault resistance.

The comparative analysis for above conditions on two area Kundur's model using FFT coefficient [22], evaluated on EVPA signal is given in Table 2. It can be seen for single fault event, the detection is achieved successfully using said method. Table 3 presents comparative analysis for multiple fault events. It is clear that FFT method shows wrong detection of event 2, means erroneous decision about the fault location. The other limitation is that FFT method does not differentiate between the lines (for double circuit line), as it treats both as single line. It detects the fault with respect to the iteration window, but not the exact instant of fault.

Performance with noise content- To validate the efficacy of proposed algorithm, the signal with noise content of 30 dB and 20 dB SNR for Case 1 & Case 2 respectively are analyzed further. The mean voltage shown in Fig. 6(a) accurately indicates the instant of fault event and its clearance. The scatter plot (HT) and TSC of LG fault near bus 7 can be clearly observed in Fig. 6(b)-(c) respectively. The changes in TSC value confirms the duration of event. Next, the analysis for multiple events (Case 2) with noise content of 20 dB is illustrated in Fig. 7. The mean voltage deviation infers accurately the instant of multiple faults and their duration as shown in Fig. 7(b).

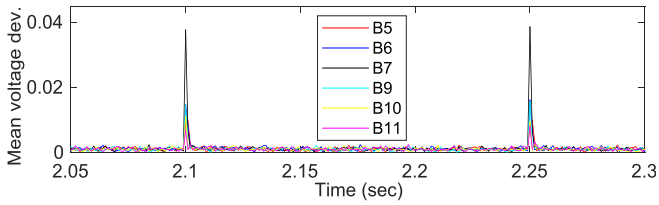

(a) Mean voltage deviation

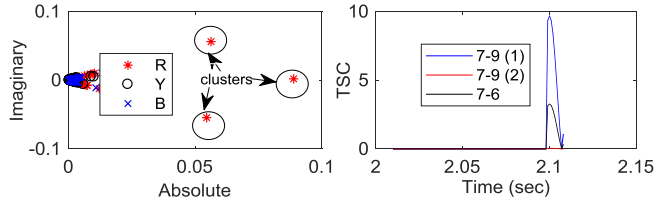

(b) LG(R-G) fault near Bus7 (c) TSC of connecting lines

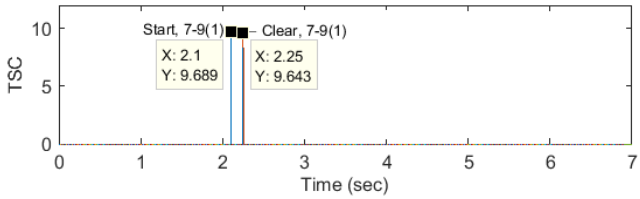

(d) Fault at line 7 - 9 (1) and its timing

Fig. 6. *Detection of fault type and its duration for Case 1 with 30 dB SNR*

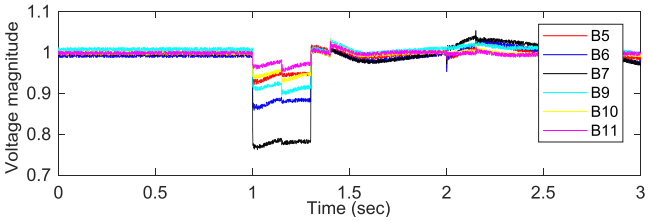

(a) Volatge magnitude of R- phase

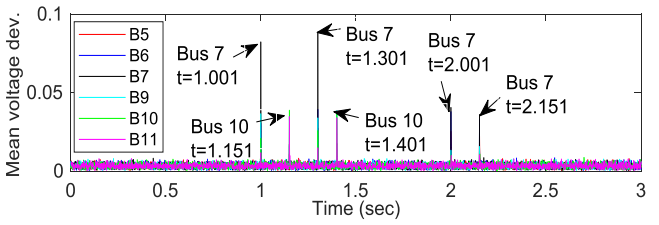

(b) Fault bus identification

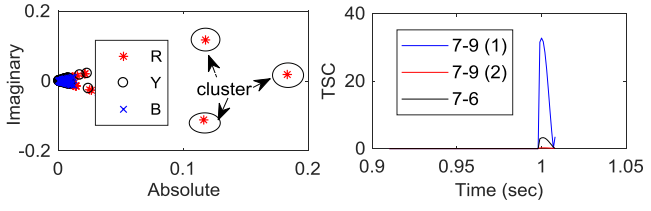

(i) First Event (LG) (ii) TSC of all lines for first event

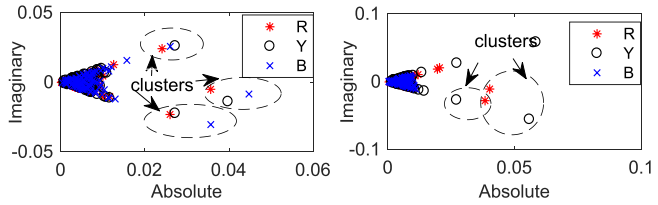

(iii) Second event (LLL) (iv) Third event (LL)

(c) Fault types detection

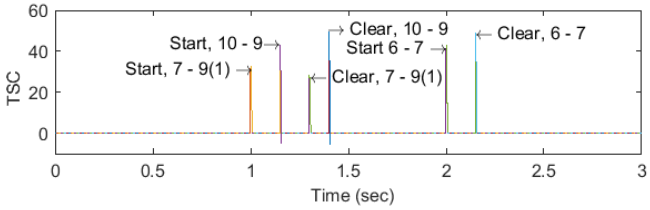

(d) Multiple faults sequence on different lines

Fig. 7. *Detection of multiple faults with 20 dB SNR*

Table 2 *Faulted bus and Faulty line detection for single event on Two area Kundur's model using FFT coefficient [22]*

Fault details	Bus	α_{100}	Faulty Bus	Connected Buses	β_{100}	Detection
(i) LG fault in 7 - 9 (1), 23 % distance from bus 7, R_f =100 Ω	5 6 **7** 9 10 11	0 0.5845 **1.204** 0.7579 0.7579 0.4517	7	**7 - 9** 7 - 6	**0.4468** 0.61995	✓
(ii) LLG fault in 6 - 7, 90 % distance from bus 6, R_f =200 Ω	5 6 **7** 9 10 11	0 0.7540 **1.5229** 0.1045 0.3219 0.5303	7	7 - 9 **7 - 6**	0.16274 **0.076882**	✓
(iii) LLL fault in 7 - 9 (2), 50 % distance from bus 7, R_f =0.001 Ω	5 6 **7** 9 10 11	0 2.8017 **4.6436** 0.2360 0.001 1.1752	7	**7 - 9** 7 - 6	**0.18418** 0.48797	✓
(v) LG fault in 9 - 10, 10 % distance from bus 9, R_f =50 Ω	5 6 7 **9** 10 11	0 0.1397 0.3441 **4.3265** 2.5950 0.6501	9	**9 - 10** 9 - 7	**0.17315** 0.39824	✓

Table 3 *Case 2: Multiple faults detection on Two area Kundur model using FFT coefficient [22]*

Event 1					Event 2					Event 3				
Bus	α_{100}	Faulty Bus	Connected Buses	β_{100}	Bus	α_{100}	Faulty Bus	Connected Buses	β_{100}	Bus	α_{100}	Faulty Bus	Connected Buses	β_{100}
5	0				5	0				5	0			
6	0.676		**9 - 7**	**0.2376**	6	0.225		7 - 9	0.5212	6	0.102		7 - 9	0.204
7	1.562		Right detection		**7**	**0.452**	7	Wrong detection		**7**	**0.204**	7	Right detection	
9	**1.586**	9			9	0.069				9	0.002			
10	1.159		9 - 10	4.269	10	0.101		**7 - 6**	**0.2262**	10	0.035		**7 - 6**	**0.101**
11	0.865				11	0.169				11	0.068			

The distinct representation of different fault types can be observed in Fig. 7(c) and TSC values in Fig. 7(d) further confirms the duration of multiple faults.

4.3 IEEE 39 bus system

This model consists of several buses interconnected to each other in a wide spread geographical area. Following cases have been considered for analysis.

Case 1: Multiple instants of fault occurrence- The following types of events are considered:

(i) First event: $LLG_{case\ 1(i)}$ fault with a fault resistance 100 Ω on line 29 - 26, at 10% distance from bus 29, occurs at t = 1 sec and clears at t = 1.27 sec.

(ii) Second event: LG [$LG_{case\ 1(ii)}$] fault with a fault resistance 10 Ω on line 4 - 14 at 50% distance from bus 4, occurs at t = 1.15 sec and clears at t = 1.35 sec.

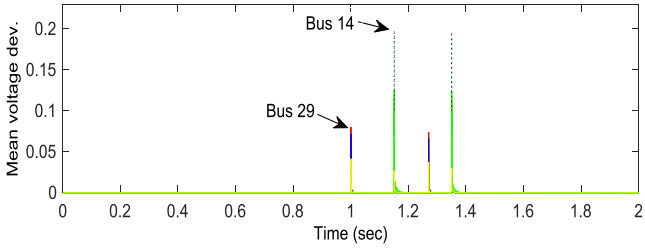

(a) Fault bus identification

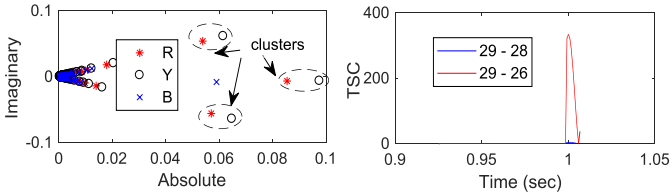

(i) First event LLG fault (RY-G phase)

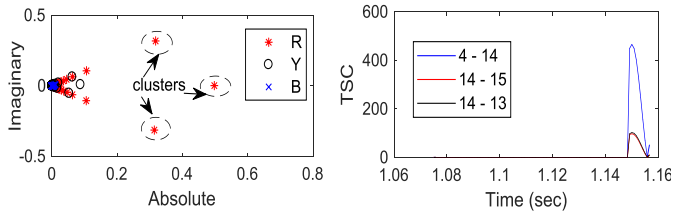

(ii) Second event LG fault (R- G phase)

(b) Fault types detection

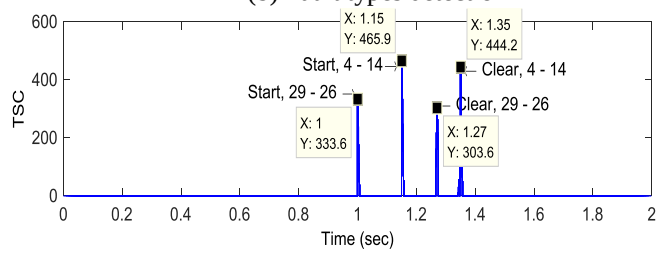

(c) Multiple faults sequence on different lines

Fig. 8. *Detection of multiple faults and its duration in IEEE39 bus system.*

In Fig. 8(a), the mean voltage deviation shows the correct sequence of fault occurrence on buses 29 & 14. This suggests that these buses share the lines associated with faults. In the single line diagram (Fig. 2(b)), bus 29 is connected to buses 26 & 28. In Fig. 8(b)(i), the HT suggests LLG fault type and TSC calculated for signals from the lines that connects these buses indicates fault occurrence on line 29 - 26. The close observation indicates that HT scatter for phases undergoing faults lie close to each other and thus in the same cluster unlike as determined for LL type (see Fig. 5(b)(iv)). Next, the second event as illustrated in Fig. 8(b)(ii) is indicated as LG fault type on line 4 - 14. A distinct cluster formation is achieved for LG or LLG for faulty phases. The performance of proposed algorithm on correctly detecting the instant of fault initiation and its clearance for fault lines can be seen in Fig. 8(c). As expected, due to initiation of multiple faults (of different types) at t = 1 sec and t = 1.15 sec leading to superposition of signals, does not actually affect the detection performance.

Case 2: Multiple instants of fault occurrence on same bus- In this case study, a given fault type is allowed to get converted into another type on the same line. Following is the description of fault occurrence.

(i) First event: LG (R-G) fault with a fault resistance 10 Ω on line 4 - 14, at 50% distance from bus 4, occurs at t = 1 sec and at t = 1.15 sec,

(ii) Second event: The above event gets converted into LLG (RY-G) type and finally clears at t = 1.35 sec. The sequence of event is indicated as $LG_{case\ 2(i)}$-$LLG_{case\ 2(ii)}$ (Fig. 2(b)).

Fig. 9(a) shows the identification of fault bus 14, with information on its occurrence. The instant at which LG fault gets converted into LLG fault at the same location is also accurately detected. Next, the scatter of HT as shown in Fig. 9(b) depicts the faults as LG and LLG with involvement of R-phase and RY-phases respectively. The detection of LLG and LG faults with distinct cluster formation for faulty phases remain consistent as discussed above. The analysis window for the signal from bus 14 with update of 10 new samples leads to the conclusion that the first event (LG type) has converted into another type (LL-G). The instant of their occurrence can be observed in Fig. 9(c). Further, to demonstrate the performance for different fault cases, Table 4 gives the computed TSC. It is clear that line undergoing fault results to have maximum value of TSC (given in bold faced) and this remains consistent irrespective of fault types, its location on the line and fault resistance.

Table 4 *TSC for all the connected lines in IEEE 39 bus system*

Fault details	Fault Bus	Connected Lines	TSC
(i) LLG fault in 26 – 29, 10% distance from bus 26, R_f =1 Ω	26	26 – 25	517.6
		26 – 27	516.7
		26 – 28	195.5
		26 - 29	**3767.8**
(ii) LG fault in 4 - 14 , 50% distance from bus 14, R_f =200 Ω	14	**4 – 14**	**9.493**
		14 – 15	2.929
		14 - 13	1.079
(iii) LG fault in 16 - 19 , 20% distance from bus 19, R_f =10 Ω	19	**19 – 16**	**1133**
		19 - 20	139.5
(iv) LL fault in 24 - 23 , 15% distance from bus 24, R_f =0.1 Ω	24	**24 – 23**	**4059**
		24 - 26	3552

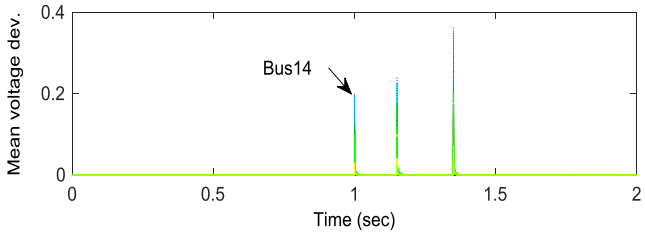

(a) Fault bus identification

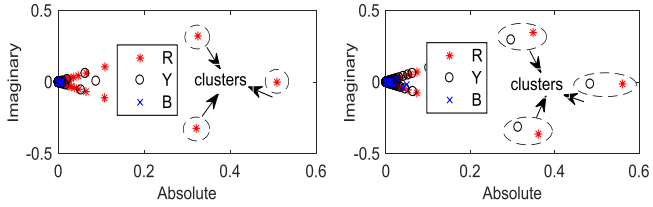

(i) LG fault (ii) LLG fault

(b) Fault types detection

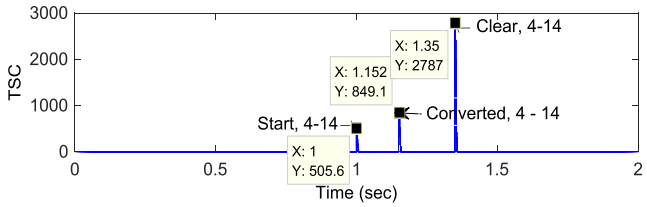

(c) Multiple faults sequence on line 4-14

Fig. 9. *Detection of multiple fault types on same bus and its duration*

Next in study, the proposed scheme is validated in real-time environment on RTDS for IEEE 39 bus system. The real-time simulation cases; case 1 and case 2 as discussed above is performed and the performance of proposed scheme is given in Table 5. The detection of faulty buses (29, 14) and lines (29-26, 14-4) for case 1 follows the same trend (Fig. 10). Similarly, in case 2, faulty bus (14) and line (14-4) are detected and this is in consistent with above discussion (Fig. 9). From Fig. 10(a), it is observed that the HT features of LLG fault (R,Y phase) can be considered in same cluster, while with LG fault (R-phase), its corresponding faulty phase separates out from the origin.

Table 5 *Fault detection on RTDS based IEEE 39 bus system*

Case	First event			Second event		
	Faulty Bus	Connected lines	TSC	Faulty Bus	Connected lines	TSC
1	29	**29 - 26** 29 - 28	**266** 98	14	14 - 13 14 - 15 **14 - 4**	189 152 **427**
2	14	14 - 13 14 - 15 **14 - 4**	199 139 **372**	14	14 - 13 14 - 15 **14 - 4**	890 678 **1818**

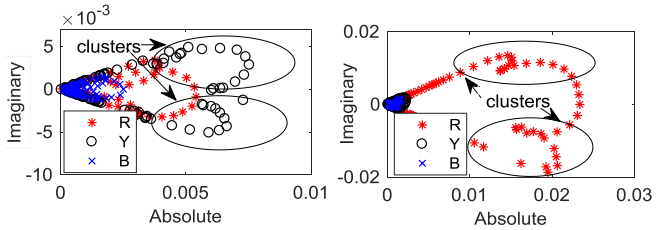

(i) LLG fault (ii) LG fault

(a) Fault types detection for case 1

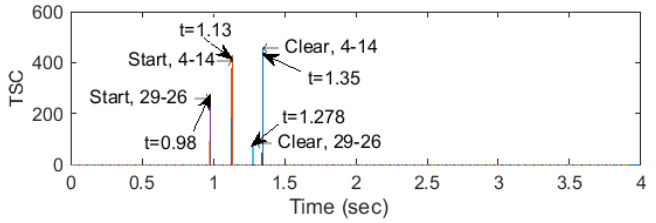

(b) Multiple faults sequence for case 1

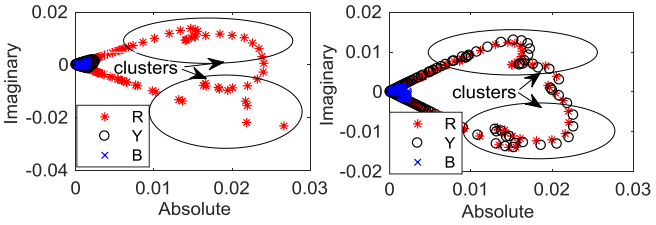

(i) LG fault (ii) LLG fault

(c) Fault types detection for case 2

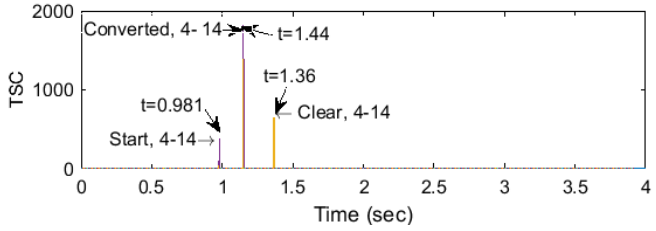

(d) Multiple faults sequence for case 2

Fig. 10. *Multiple fault event detection on real time simulation*

The peak of TSC shown in Fig. 10(b) indicates the instant of multiple faults occurrence. Next, in Fig. 10(c) & (d), consistent results are indicated in view of identification of fault types and its sequence.

The performance of proposed algorithm satisfactorily concludes about its application in real-time. It is obvious that, real-time measurement includes most dynamics of system and thus transient signals. As a result, for the same fault duration and sequence, more number of HT features are separated out and lie within the same cluster unlike simulated results having only one feature in each cluster (Fig. 5-9).

5 Conclusion

The paper presented computationally reliable method for detection of instant of multiple faults and its types. The algorithm was applied on 100 samples window with 90% overlap for complete length of signal, suggesting a frame of only 10 new samples in analysis for detection of fault instant and its type. In the first step, the signals available via PMUs were processed and subsequently TF representation was obtained using SPWVD technique. The calculation of indices from TF representation successfully interpretated the fault events. The calculation of change in TF spectra and TSC were capable to accurately indicate the instant of subsequent events of fault occurrence on the line. The representation of scattered plots of absolute and imaginary components, calculated using Hilbert transform was helpful in suggesting the fault types.

The proposed scheme was demonstrated on simulated signals for multiple faults events on standard bus system with and without noise and as well as for real time measurements. In other words, the sequence of LLG and LG faults, before the clearance of former event, on different lines were accurately detected and discriminated. Also, the sequence of LG fault converting into LLG fault, before the clearance of former event, on the same line was successfully detected in study. The novelty of the proposed approach lies in the fact that proposed scheme was able to detect the fault location within 10msec, and instead of analysing all the lines, only connected buses from the faulty bus were analysed for detection of the faulty line. It reduces the computational strain.

6 Acknowledgment

The financial support received from joint Indo-Norway (DST-RCN) project collaboration.

7 References

[1] Liang, X., Wallace, S.A., Zhao, X.: 'A technique for detecting wide area single-line-to-ground faults', IEEE Conf. Technol. Sustain., 2014, pp. 121-124.

[2] Tayeb, E.B.M., A Rhirn, O.A.A.: 'Transmission line faults detection, classification and location using artificial neural network', Int. Conf. Utility Exhib. Power Energy Syst., Issues Prospects Asia, 2011, pp. 1-5.

[3] Sachdev, M.S., Das, R., Sidhu, T.S.: 'Determining locations of faults in distribution systems', in Proc. Dev. Power Syst. Protection, 1997, pp. 188-191.

[4] Yusuff, A.A., Jimoh, A.A., Munda, J.L.: 'Determinant-based feature extraction for fault detection and classification for power transmission lines', IET Gener. Transm. Distrib., 2011, 5, (12), pp. 1259-1267.

[5] Jafarian, P., Sanaye-Pasand, M.: 'A traveling-wave-based protection technique using wavelet/PCA analysis', IEEE Trans. Power Del., 2010, 25, (2), pp. 588-599.

[6] Liu, Z., Han, Z., Zhang, Y., Zhang, Q.: 'Multiwavelet packet entropy and its application in transmission line fault recognition and classification', IEEE Trans. Neural Netw. Learn. Syst, 2014, 25, (11), pp. 2043-2052.

[7] Upendar, J., Gupta, C.P., Singh, G.K.: 'Statistical decision-tree based fault classification scheme for protection of power transmission lines', Electrical Power and Energy Systems, 2012, 36, (1), pp. 1-12.

[8] Upendar, J., Gupta, C.P., Singh, G.K., Ramakrishna, G.: 'PSO and ANN-based fault classification for protective relaying', IET Gener. Transm. Distrib., 2010, 4, (10), pp. 1197-1212.

[9] Hasheminejad, S., Seifossadat, S.G., Razaz, M., Joorabian, M.: 'Traveling-wave based protection of parallel transmission lines using Teager energy operator and fuzzy systems', IET Gener. Transm. Distrib., 2016, 10, (4), pp. 1067-1074.

[10] Yadav, A., Swetapadma, A.: 'Enhancing the performance of transmission line directional relaying, fault classification and fault location schemes using fuzzy inference system', IET Gener. Transm. Distrib., 2015, 9, (6), pp. 580-591.

[11] Biswal, M.: 'Faulty phase selection for transmission line using integrated moving sum approach', IET Sci. Meas. Technol., 2016, 10, (7), pp. 761-767.
[12] Korkali, M., Lev-Ari, H., Abur, A.: 'Traveling-Wave-Based Fault-Location Technique for Transmission Grids Via Wide-Area Synchronized Voltage Measurements', IEEE Transactions On Power Systems, May 2012, 27, (2), pp 1003-1011.
[13] Guillen, D., Paternina, M.R.A, Zamora, A., Ramirez, J.M., Idarrage, G.: 'Detection and classification of faults in transmission lines using the maximum wavelet singular value and Euclidean norm', IET Generation, Transmission & Distribution,2015, 9 (15), pp 2294-2302.
[14] Das, S., Singh, S.P., Panigrahi, B.K.: 'Transmission line fault detection and location using Wide Area Measurements', Electrical Power Systems Research, May 2017, 151, pp. 96 -105.
[15] Roy, B.K.S., Sharma, R., Pradhan, A.K.; "Faulty line Identification algorithm for secured backup protection using PMUs," Electrical Power Component and Systems, 2017, 0, (0), 1-14.
[16] Rajaraman, P., Sandaravaradan, N.A., Mallikarjuna, B., Jaya, B. R. M. et al.: "Robust fault analysis in transmission lines using Synchrophasor measurements," Protection and Controls of Modern Power System, June 2018, 3, (14), pp. 1-13.
[17] Yu, F., Booth, C., Dysko, A. Hong, Q.: "Wide area backup protection and protection performance analysis scheme using PMU data," International Journal of Electrical Power and Energy Systems, 2019, 110, pp. 630-641.
[18] Li, Z., Yin, X., Zhang, Z., He, Z.: 'Wide-area protection fault identification algorithm based on multi-information fusion', IEEE Trans. Power Del.,2013, 28, (3), pp 1348-1355.
[19] Nayak, P.K., Pradhan, A.K., Bajpai, P.: 'Wide-area measurement-based back up protection for power network with series compensation', IEEE Trans. Power Del., Jan 2014, 29, (4), pp 1970-1977.
[20] Dubey, R., Samantaray, S.R., Panigrahi, B.K.: 'An spatiotemporal information system based wide-area protection fault identification scheme', Electrical Power and Energy System, July 2017, 89, pp 136-145.
[21] Liang, X., Wallace, S.A., Nguyen, D.: 'Rule-Based Data-Driven Analytics for Wide-Area Fault Detection Using Synchrophasor Data', IEEE Transactions on Industry Applications, June 2017, 53, (3), pp 1789-1798.
[22] Gopakumar, P., Reddy, M.J.B., Mohanta, D.K.: 'Transmission line fault detection and localisation methodology using PMU measurements', IET Gener. Transm. Distrib., 2015, 9, (11), pp. 1033–1042.
[23] Guillen. D., Paternina. M.R.A., Bejar., J.O. et al: 'Fault detection and classification in transmission lines based on a PSD index', IET Generation, Transmission & Distribution, 2018, 12 (18), pp. 4070-4078.
[24] Ndreko, M., Van der Meer, A.A, Gibescu, M., Van der Meijden, M.A.M.M.: 'Impact of DC voltage control parameters on AC/DC system dynamics under faulted conditions',*2014 IEEE PES General Meeting Conf. Expo.*, National Harbor, MD, 2014, pp 1-5.
[25] Paternina., M.R.A., Mendez., A.Z., Bejar., J.O., Chow., J.H., et al.: 'Identification of coherent trajectories by modal characteristics and hierarchical agglomerative clustering', Electric Power Systems Research, 2018, 158, 170-183.
[26] Flandrin, P.: 'Time-Frequency/Time-Scale Analysis' (New York: Academic, Ed., 1999).
[27] Orini, M., Bailon, R., Mainardi, L.T., et al.: 'Characterization of dynamic interactions between cardiovascular signals by time–frequency coherence', IEEE Trans. Biomed. Eng., 2012, 59, (3), pp. 663–673.
[28] Costa, A.H, Boudreau-Bartels, G.F.: "Design of time-frequency representation using a multiform, tiltable exponential kernel," IEEE Trans. Signal Process., Oct. 1995, 43, (10), pp. 2283–2301
[29] Kundur, P.: 'Power system stability and control' (Tata McGraw-Hill Education Pvt. Ltd., New Delhi, 2012).
[30] Ackermann, T.: 'Wind power in power systems' (Wiley & Sons Ltd, Chichester, UK, 2005).